



This is the accepted manuscript made available via CHORUS. The article has been published as:

Quantum efficiency of a single microwave photon detector based on a semiconductor double quantum dot

Clement H. Wong and Maxim G. Vavilov

Phys. Rev. A **95**, 012325 — Published 24 January 2017

DOI: [10.1103/PhysRevA.95.012325](https://doi.org/10.1103/PhysRevA.95.012325)

Quantum efficiency of a single microwave photon detector based on a semiconductor double quantum dot

Clement H. Wong

Laboratory for Physical Sciences, University of Maryland, College Park, Maryland 20740, USA

Maxim G. Vavilov

Department of Physics, University of Wisconsin-Madison, Madison, Wisconsin 53706, USA

(Dated: January 3, 2017)

Motivated by recent interest in implementing circuit quantum electrodynamics with semiconducting quantum dots, we consider a double quantum dot (DQD) capacitively coupled to a superconducting resonator that is driven by the microwave field of a superconducting transmission line. We analyze the DQD current response using input-output theory and show that the resonator-coupled DQD is a sensitive microwave single photon detector. Using currently available experimental parameters of DQD-resonator coupling and dissipation, including the effects of $1/f$ charge noise and phonon noise, we determine the parameter regime for which incident photons are completely absorbed and near unit $\gtrsim 98\%$ efficiency can be achieved. We show that this regime can be reached by using very high quality resonators with quality factor $Q \simeq 10^5$.

I. INTRODUCTION

High performance, single photon detectors are essential tools in quantum optics, with applications in optical quantum information processing, communication, cryptography, and metrology [1]. Single photon detection in the microwave regime has similar applications in the emerging field of microwave quantum photonics, made possible by recent advances in implementing circuit quantum electrodynamics (cQED) with superconducting circuit technology [2, 3], but are more difficult to achieve because microwave photons have energy five orders of magnitude less than optical photons. Besides photonics, microwave photon detectors have applications in astronomy and cosmology, for example, in measuring the cosmic microwave background [4]. Microwave radiometers are commonly used in meteorological and oceanographic remote-sensing.

Recent theoretical proposals and experimental developments in microwave photon detectors include those based on Josephson junctions [5–10], and optoelectromechanical systems [11–13]. At the same time, experimental progress in implementing cQED with semiconducting quantum dots is showing promise [14–24]. Currently available resonator-quantum dot systems already allow for some interesting quantum optics applications such as on-chip single emitter masers [25, 26], and tunable self-interaction and dissipation of the resonator photons induced by the quantum dot [27, 28]. When a quantum dot is connected to electric leads, this system provides a platform for studying the interplay between quantum impurity physics and quantum optics [29].

In this paper, we propose a photon detector based on photon assisted tunneling of electrons through a double quantum dot (DQD), and determine the quantum efficiency of single photon detection. We identify the parameter regime where reflection of input photons from the resonator vanishes, so that near unit efficiency can be

achieved with currently available experimental parameters. Such a high efficiency is possible even in the presence of strong DQD dissipation because the detection process takes advantage of fast dot-lead tunneling relative to the DQD inelastic decay rate, and does not require strong DQD-resonator coupling relative to the DQD dissipation rates. The photon detector utilizes only charge states of the DQD and does not require magnetic fields that would degrade the quality factor of the superconducting resonator cavities.

The zero reflection regime is also relevant in the context of quantum computation, since it enables distant transmission of quantum information required in quantum cryptography and communication [30, 31]. We also note that when the input photons come from a hot thermal source, this device acts as a quantum heat engine [32, 33].

This paper is organized as follows. In Sec. II, we introduce our theoretical model for the transmission line carrying incoming photons and the photon detector. In Sec. III, we present the equations of motion governing the system dynamics, and in Sec. IV, we present the steady state solution, which is used to derive an analytic expression for the quantum efficiency of photon detection in Sec. V. In Sec. VI, we discuss how the reflected signal is incorporated in our model, and in Sec. VII, we find the optimal parameter regime. A brief summary of the decoherence model we used for the DQD is given in the appendix.

II. MODEL

We consider a microwave photon detector consisting of a superconducting microwave resonator coupled to a DQD, which receives photons from a semi-infinite microwave transmission line, as shown in Fig. 1. The DQD is operated in the “pumping” configuration, with zero source-drain bias and near the charge tran-

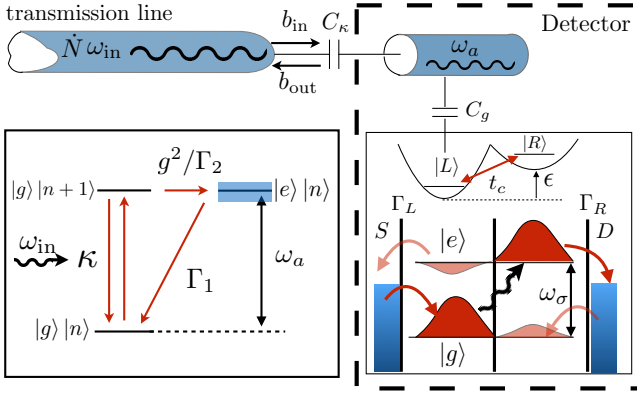


FIG. 1. (Color online) Top left: A transmission line carries a continuous wave of microwave photons with flux \dot{N} and frequency ω_{in} . Right dashed box: The photon detector is a single port superconducting resonator with frequency ω_a , capacitively coupled to a double quantum dot (DQD) with a coupling g . The DQD is set to zero source-drain bias, with the lead chemical potentials set in between the ground and excited state. Absorption of a resonator photon cause transitions between the DQD states $|g\rangle$ and $|e\rangle$, resulting in current flow. Lower left box: Energy levels (horizontal lines) and transition processes (single directed arrows) in the resonator-DQD system. A single photon received by the resonator ($|g\rangle|n+1\rangle$) can be emitted at the rate κ or be absorbed by the DQD at the rate g^2/Γ_2 , exciting the metastable state $|e\rangle|n\rangle$ and then decaying back to the system ground state $|g\rangle|n\rangle$ at the inelastic decay rate Γ_1 .

sition between the charge states $|L\rangle = |N+1, M\rangle$ and $|R\rangle = |N, M+1\rangle$, where $|N, M\rangle$ denotes N (M) electrons in the left (right) dot. The electron Hamiltonian governing behavior of the dot with $M+N+1$ electrons is

$$H_{\text{DQD}} = \hbar \frac{\epsilon \tau_z + 2t_c \tau_x}{2} = \frac{\hbar \omega_\sigma \sigma_z}{2}, \quad (1)$$

where $\tau_{x,z}$ are the Pauli matrices in the charge basis, $|L, R\rangle$, while $\sigma_z = |e\rangle\langle e| - |g\rangle\langle g|$ is the diagonal Pauli matrix in the basis of eigenstates of H_{DQD} :

$$\begin{pmatrix} |g\rangle \\ |e\rangle \end{pmatrix} = \begin{pmatrix} \cos \frac{\theta}{2} & -\sin \frac{\theta}{2} \\ \sin \frac{\theta}{2} & \cos \frac{\theta}{2} \end{pmatrix} \begin{pmatrix} |L\rangle \\ |R\rangle \end{pmatrix} \quad (2)$$

We introduced the following notations: ϵ is the DQD voltage bias across the dots, counted from the charge degeneracy point, t_c is the interdot tunnel coupling, and $\omega_\sigma = \sqrt{4t_c^2 + \epsilon^2}$ is the DQD excitation energy and $\cos \theta = -\epsilon/\omega_\sigma$.

We consider zero bias across the leads, when electrons in the excited state can tunnel out incoherently to the leads, resulting in the “empty” state $|0\rangle = |N, M\rangle$, and then, the ground state $|g\rangle$ can be loaded by electron tunneling from the leads. The Hamiltonian describing tun-

neling to the leads is given by

$$H_\Gamma = \sum_{i=L,R} \sum_{\mathbf{k}} \left(\epsilon_{\mathbf{k}} c_{i\mathbf{k}}^\dagger c_{i\mathbf{k}} + t_i c_{i\mathbf{k}}^\dagger d_i + t_i^* c_{i\mathbf{k}} d_i^\dagger \right),$$

where $d_i^\dagger = |i\rangle\langle 0|$, $c_{i\mathbf{k}}^\dagger = |\mathbf{k}\rangle\langle i|$, $\epsilon_{\mathbf{k}}$ is the dispersion for an electron state $|\mathbf{k}\rangle$ with wave vector \mathbf{k} in the leads and $|i\rangle$ is a state in the L/R dot. The resulting incoherent tunneling rates from $|e\rangle$ to $|0\rangle$ (Γ_{0e}) and from $|0\rangle$ to $|g\rangle$ (Γ_{g0}) are given by [19, 20, 34]

$$\Gamma_{0e} = \Gamma_L \cos^2(\theta/2) + \Gamma_R \sin^2(\theta/2), \quad (3a)$$

$$\Gamma_{g0} = \Gamma_L \sin^2(\theta/2) + \Gamma_R \cos^2(\theta/2), \quad (3b)$$

where $\Gamma_{R(L)}$ are tunneling rates to the right (left) leads.

Taking into account opposite currents due to loading from and tunneling to the leads, the time-averaged electron current through the DQD can be written as

$$\langle I \rangle = e \Gamma_R \{ \langle p_e \rangle |\langle R|e\rangle|^2 - \langle p_0 \rangle |\langle R|g\rangle|^2 \}, \quad (4)$$

where $p_\alpha = |\alpha\rangle\langle\alpha|$ is the projection operator to state $|\alpha\rangle$, $\langle \dots \rangle$ denotes the quantum mean value and time average.

In the absence of photon excitation of the dot and at temperature $T=0$, the DQD is in the ground state, $\langle p_g \rangle = 1$ and $\langle p_e \rangle = \langle p_0 \rangle = 0$, and no current flows. However, photons in the microwave resonator cause transitions between the ground and excited states of the DQD, which enables sequential tunneling $(N, M) \rightarrow (N+1, M) \rightarrow (N, M+1)$, resulting in a finite current. Photon arrivals can thus be detected by measuring the DQD source-drain current. We note that, because the DQD is operated in the limit of relatively strong coupling to the leads, spin is not conserved [35] and the spin blockade does not occur in the proposed device. At finite temperature, the tunneling rates Eq. (3a) and Eq. (3b) should be modified with appropriate Fermi functions for the leads. When thermal broadening in the leads becomes comparable to the photon energy, there can be a back current due to electrons that tunnel from the lead to the excited state, emit a photon followed by the transition to the ground state, and then tunneling from the ground state to the lead. However, this effect is negligible at an operating temperature of 40 mK = 0.8 GHz \hbar/k_B , an order of magnitude lower than the photon energy we consider.

The Hamiltonian of non-interacting photons and the DQD in the rotating frame at the frequency of input photons ω_{in} are

$$H_{\text{free}} = \int_{-\infty}^{\infty} \frac{d\omega}{2\pi} \hbar \omega b_\omega^\dagger b_\omega + \hbar \Delta_{ab} \left(a^\dagger a + \frac{1}{2} \right), \quad (5)$$

$$\tilde{H}_{\text{DQD}} = \frac{\hbar \Delta_{\sigma b}}{2} \sigma_z. \quad (6)$$

where $\Delta_{ab} = \omega_a - \omega_{\text{in}}$ ($\Delta_{\sigma b} = \omega_\sigma - \omega_{\text{in}}$) is the detuning of the resonator frequency (DQD) ω_a (ω_σ) from ω_{in} .

Here, we used the mode expansions

$$V_{\text{TL}} = \int_{-\infty}^{\infty} \frac{d\omega}{2\pi} \sqrt{\frac{\hbar\omega Z_{\text{TL}}}{2}} (b_{\omega} + b_{\omega}^{\dagger}) . \quad (7)$$

$$V_a = \sqrt{\frac{\hbar\omega_a}{2C_a}} (a + a^{\dagger}) , \quad (8)$$

for the resonator (V_a) and transmission line (V_{TL}) voltage operator at the coupling capacitor C_{κ} , where a is the resonator photon annihilation operator and b_{ω} is the transmission line photon annihilation operator with frequency ω [36]. Furthermore, $Z_{\text{TL}} = \sqrt{l/c}$ is the characteristic impedance of the line, l is the inductance per unit length, c is the capacitance to ground per unit length, and C_a is resonator capacitance. We assume the transmission line dispersion $\omega_k = vk$, where $v = 1/\sqrt{lc}$ is the group velocity.

The resonator-DQD coupling is described by the Jaynes-Cummings Hamiltonian:

$$H_{\text{JC}} = \hbar g (\sigma^{\dagger} a + a^{\dagger} \sigma), \quad (9)$$

where $\sigma = |g\rangle\langle e|$ is the DQD lowering operator. Here, the interaction strength $g = g_0 \sin \theta$ is defined by the dipole matrix element in the basis of energy eigenstates, and

$$g_0 = \omega_a \beta_g \sqrt{\frac{\pi Z_a}{R_Q}} ,$$

where Z_a is the resonator characteristic impedance, $R_Q = h/2e^2 = 12.9 \text{ k}\Omega$ is the resistance quantum, $\beta_g = C_g/(C_g + C_{\Sigma})$, C_g is the gate capacitance between the resonator and the DQD, and C_{Σ} is the total capacitance of the DQD [24].

The photon mode in the resonator is driven by photons exchange with the transmission line. Assuming a weak, local coupling capacitance C_{κ} between transmission line photons and the resonator, the interaction Hamiltonian in the rotating wave approximation is given by

$$H_{\text{TL}} = C_{\kappa} V_a V_{\text{TL}} = \hbar \sqrt{\kappa} \int \frac{d\omega}{2\pi} [b_{\omega}^{\dagger} a + a^{\dagger} b_{\omega}], \quad (10a)$$

where

$$\kappa = C_{\kappa}^2 \omega_{\text{in}}^3 \frac{Z_{\text{TL}} Z_a}{4} , \quad (10b)$$

is the photon leakage rate from the resonator, $Z_a = \sqrt{L_a/C_a}$ is the impedance of the coplanar waveguide resonator, and L_a is the resonator inductance. We notice that the resonator quality factor can be expressed as

$$Q = \frac{\omega_{\text{in}}}{\kappa} = \frac{4Z_{\text{TL}}}{Z_a (\omega_{\text{in}} \tau_{\text{RC}})^2}$$

where $\tau_{\text{RC}} = C_{\kappa} Z_{\text{TL}}$ is the recharging time of the coupling capacitor C_{κ} .

To finalize the description of the model, we present the full Hamiltonian of the system:

$$H = H_{\text{sys}} + H_{\text{TL}} + H_{\Gamma} + H_{\gamma} \quad (11a)$$

$$H_{\text{sys}} = \tilde{H}_{\text{DQD}} + H_{\text{JC}} + H_{\text{free}} , \quad (11b)$$

In Eq. (11a), H_{γ} is the Hamiltonian describing the DQD dissipative environment, which consist of voltage fluctuations and phonons.

III. EQUATIONS OF MOTION

We will employ input-output theory [37–40] to model the resonator-transmission line interaction. This formalism will enable us to optimize the quantum efficiency of photon detection including interference effects between the microwave signals reflected by the resonator-DQD system, which is not captured by density matrix master equations. The key assumptions in this formalism is the rotating wave and Markov approximation.

The equation of motion for the transmission line modes that follows from the Hamiltonians in Eq. (10a) and Eq. (5) can be solved analytically to yield

$$b_{\omega}(t) = e^{-i\omega(t-t_0)} b_{\omega}(t_0) + i\sqrt{\kappa} \int_{t_0}^t dt' e^{-i\omega(t-t')} a(t') \quad (12)$$

which is a solution that can be specified by initial $t_0 = t_i < t$ or final condition $t_0 = t_f > t$, at time t_i (t_f) long before (after) the transmission line photons interact with the resonator. The input field in the rotating frame is defined by the initial field configuration as

$$b_{\text{in}}(t) = \int_{-\infty}^{\infty} \frac{d\omega}{2\pi} b_{\omega}(t_i) e^{-i\omega(t-t_i)} . \quad (13)$$

We will consider the case where the input field is formed by a continuous flux of photons in a narrow spectral band around ω_{in} , corresponding to the initial state [41]

$$|\beta_i\rangle = \frac{1}{\sqrt{n_b!}} \left[\int d\omega f(\omega) b_{\omega}^{\dagger}(t_i) \right]^{n_b} |0\rangle_{\text{TL}}$$

where $|f(\omega)|^2 = \delta(\omega - \omega_{\text{in}})$ and $|0\rangle_{\text{TL}}$ is the vacuum state of the transmission line. The flux of incoming photons is given by the expectation value in $|\beta_i\rangle$, $\dot{N} = \langle b_{\text{in}}^{\dagger}(t) b_{\text{in}}(t) \rangle$. In terms of experimental parameters, $\dot{N} = v n_b / L = n_b / Z_{\text{TL}} c L$, where n_b is total input photon number of the waveguide and the transmission line impedance is $Z_{\text{TL}} = 50\Omega$.

Using the solution Eq. (12) specified by b_{in} leads to the Heisenberg-Langevin equations for the system operators $\{X\} = \{a, \sigma, \sigma_z, p_0\}$ given by [37, 39, 40]

$$\begin{aligned} \dot{X} = & \frac{i}{\hbar} [H_{\text{sys}}, X] + (D_{\gamma} + D_{\Gamma}) X \\ & + (\kappa/2 - i\sqrt{\kappa} b_{\text{in}}^{\dagger}) [X, a] + [a^{\dagger}, X] (\kappa/2 + i\sqrt{\kappa} b_{\text{in}}) \end{aligned} \quad (14)$$

where $\mathcal{D}(A)$ is the Linblad superoperator defined by $\mathcal{D}(A)\rho = A\rho A^\dagger - (A^\dagger A\rho + \rho A^\dagger A)/2$. Here, D_Γ is the dissipative operator describing incoherent tunneling to the leads, given by

$$D_\Gamma = \Gamma_{0e}\mathcal{D}(|0\rangle\langle e|) + \Gamma_{g0}\mathcal{D}(|g\rangle\langle 0|). \quad (15)$$

Other incoherent processes in the dynamics of the DQD originate from interaction of charge degrees of freedom of the DQD with its environment, such as the phonon system and charge noise in dielectric. The DQD charge coupling to phonons is similar to the coupling to the resonator field, see Appendix A1 and Refs. [19, 42, 43]. The charge noise results in an additional component $\delta\epsilon(t)$ of the bias between the dots, $\epsilon \rightarrow \epsilon + \delta\epsilon(t)$, this noise typically exhibits a $1/f$ power spectrum, see Appendix A2. The Linblad superoperator D_γ accounts for these incoherent processes

$$D_\gamma = \gamma_\uparrow(\epsilon)\mathcal{D}(\sigma^\dagger) + \gamma_\downarrow(\epsilon)\mathcal{D}(\sigma). \quad (16)$$

Here, $\gamma_\uparrow(\epsilon)$ and $\gamma_\downarrow(\epsilon)$ are the bias dependent excitation and relaxation rates, respectively. We describe contributions to these rates from electron-phonon interaction and high frequency component of the charge noise in Appendix A1 and A2.

From Eq. (14) and Eq. (15), the equations of motion for the photon and DQD operators are [37]

$$\dot{a} = -\left(\frac{\kappa}{2} + i\Delta_{ab}\right)a - ig\sigma + i\sqrt{\kappa}b_{\text{in}} \quad (17a)$$

$$\dot{\sigma} = -(\Gamma_2 + i\Delta_{\sigma b})\sigma + ig a\sigma_z \quad (17b)$$

where

$$\Gamma_2 = \frac{\gamma_1 + \Gamma_{0e}}{2} \quad (18)$$

is the transverse relaxation rate, which includes incoherent dynamics of the DQD between states $|e\rangle$ and $|g\rangle$ with the combined rate $\gamma_1 = \gamma_\uparrow + \gamma_\downarrow$ and lifetime broadening due to incoherent tunneling to the leads at the rate Γ_{0e} , Eq. (3a).

The low frequency component of charge $1/f$ noise causes non-Markovian dynamics, which strictly speaking, should be described by a nonlocal damping kernel in Eq. (17b) of the form $\dot{\sigma} = -(\Gamma_2 + \int_0^t dt' \Sigma(t-t'))\sigma(t') + \dots$ [44], where $\Sigma(t) = \gamma_\phi \omega_l e^{-\omega_l t}$, ω_l being the noise correlation time, and γ_ϕ can be estimated with the pure dephasing rate given in Eq. (A7). However, we will only need the steady state solution, which is determined by the zero mode in the Laplace transform of the equations of motion. This zero mode equation is consistent with Eq. (17b) with the total damping rate $\Gamma_2 + \gamma_\phi$ where $\gamma_\phi = \int_0^\infty dt \Sigma(t)$ is the zero mode component of the damping kernel. Thus, to take into account low frequency $1/f$ type noise in our proposed device, it is sufficient to take $\Gamma_2 \rightarrow \Gamma_2 + \gamma_\phi$, where γ_ϕ is given by Eq. (A7) of Appendix A2.

We note that it has been established both experimentally and theoretically that noise in the DQD bias ϵ is

much stronger than tunnel coupling noise, and in most cases, DQD decoherence can be modeled by only ϵ noise [45, 46]. Furthermore, our device operates in the regime $\epsilon \gtrsim t_c$, where the DQD frequency depends very weakly on t_c , so that any dephasing due to noise in t_c is strongly suppressed. Finally, we note that since we are not detecting the quantum state of the photon, details of the DQD coherence is not of central importance. As we will show below in Eq. (36), the decoherence rate Γ_2 can change the optimal parameter regime but does not necessarily limit performance, since the resonator leakage rate κ can be adjusted to maintain the optimal condition.

The equations of motion the DQD polarization and “empty” state projection operators are

$$\dot{\sigma}_z = 2ig(a^\dagger\sigma - \sigma^\dagger a) \quad (19a)$$

$$+ \left(\gamma_- - \frac{\Gamma_{0e}}{2}\right)p_\sigma - \left(\gamma_1 + \frac{\Gamma_{0e}}{2}\right)\sigma_z - p_0\Gamma_{g0},$$

$$\dot{p}_0 = \Gamma_{0e}\frac{p_\sigma + \sigma_z}{2} - \Gamma_{g0}p_0 \quad (19b)$$

where $p_\sigma = |e\rangle\langle e| + |g\rangle\langle g|$ is the projection operator into the charge qubit subspace, determined by the constraint the $p_0 + p_\sigma = |e\rangle\langle e| + |g\rangle\langle g| + |0\rangle\langle 0| = 1$, which represent conservation of probability in the DQD state space.

IV. STEADY-STATE SOLUTION

We will compute the detection efficiency for the case of continuous flux of photons using the steady state solution to the equations of motion [1]. Here, we present the steady state solution for the polarization $m_z \equiv \langle\sigma_z\rangle$, for a purely quantum input field with zero classical component $\langle b_{\text{in}}\rangle = 0$, and then relate m_z to the detection efficiency of the device [47].

We eliminate the “empty” dot operator p_0 using the steady state solution of Eq. (19b), which yields

$$p_\sigma = \frac{2\Gamma_{g0} - \Gamma_{0e}\sigma_z}{\Gamma_{0e} + 2\Gamma_{g0}}. \quad (20)$$

Then, substituting Eq. (20) to Eq. (19a) yields an effective equations of motion for the polarization

$$\dot{m}_z = \Gamma_1(m_0 - m_z) + 2ig\langle a^\dagger\sigma - \sigma^\dagger a \rangle, \quad (21a)$$

$$\Gamma_1 = \gamma_1 + \frac{2\Gamma_{0e}\Gamma_{g0} - \gamma_s\Gamma_{0e}}{\Gamma_{0e} + 2\Gamma_{g0}} \quad (21b)$$

$$m_0 = -\frac{(\gamma_s + \Gamma_{0e})\Gamma_{g0}}{(\gamma_1 + \Gamma_{0e})\Gamma_{g0} + \Gamma_{0e}(\gamma_1 - \gamma_s)/2} \quad (21c)$$

where Γ_1 is the effective depolarization rate and $\gamma_s = \gamma_\downarrow - \gamma_\uparrow$ is the phonon-induced spontaneous emission rate, cf. Eq. (16).

At this point, the three level DQD system consisting of $\{|e\rangle, |g\rangle, |0\rangle\}$ is reduced to a two level system described by Eqs. (17b) and (21a) with longitudinal and transverse

relaxation rates Γ_1 and Γ_2 , respectively. The equilibrium polarization m_0 gives the value of m_z in the absence of coupling to resonator photons, $g = 0$. The effective DQD excitation, relaxation, and dephasing rates are $\Gamma_\uparrow = \Gamma_1(1 + m_0)/2$ and $\Gamma_\downarrow = \Gamma_1(1 - m_0)/2$, and $\Gamma_\phi = \Gamma_2 - \Gamma_1/2$, respectively.

The steady state photon and DQD operators satisfy

$$a = \chi_a(\sqrt{\kappa}b_{\text{in}} - g\sigma) \quad (22a)$$

$$\sigma = g\chi_\sigma(a\sigma_z) \quad (22b)$$

where $\chi_a = (\Delta_{ab} - i\kappa/2)^{-1}$ and $\chi_\sigma = (\Delta_{\sigma b} - i\Gamma_2)^{-1}$ are the resonator and DQD susceptibilities [40]. To solve these equations, we apply the mean field approximation to Eq. (22b) by taking $a\sigma_z \rightarrow am_z$, and substitute Eq. (22b) into Eq. (22a) to find the resonator photon field

$$a = \chi_{ab}b_{\text{in}}, \quad (23a)$$

$$\chi_{ab} = \frac{\sqrt{\kappa}}{\Delta_{ab} - i\kappa/2 + g^2m_z\chi_\sigma}. \quad (23b)$$

This solution, together with the steady state solution of Eq. (21a) yields the mean field equation

$$m_z = \frac{m_0}{1 + G\langle n_a \rangle}, \quad (24a)$$

$$\langle n_a \rangle = |\chi_{ab}|^2 \langle b_{\text{in}}^\dagger b_{\text{in}} \rangle, \quad (24b)$$

where $G = (4g^2/\Gamma_1)\text{Im}\chi_\sigma$ and $n_a = a^\dagger a$ is the resonator photon number operator.

Due to the dependence on m_z in Eq. (23b), the mean field equation (24a) is a cubic equation for m_z [39]. However, a simple estimate based on the perturbative parameter $G \leq g^2/\Gamma_1\Gamma_2 \simeq 10^{-4}$ will show that it is sufficient to take $m_z = m_0$ in Eq. (23b), so that Eq. (24a) yields explicit solution for m_z . The photon-induced polarization is

$$\Delta m_z = m_z - m_0 = -m_0 \frac{G\langle n_a \rangle}{1 + G\langle n_a \rangle}, \quad (25)$$

which, to leading order yields $\Delta m_z \approx |m_0|G\langle n_a \rangle \simeq G\dot{N}/\kappa$, where we kept $\langle n_a \rangle \simeq \dot{N}/\kappa$ to $\mathcal{O}(1)$. Substituting this in Eq. (23b) yields the leading order correction to the photon number $\langle \Delta n_a \rangle \simeq CG(\dot{N}/\kappa)^2$, where

$$C = g^2/\Gamma_2\kappa \quad (26)$$

is the cooperativity. As shown in section V, $C = \mathcal{O}(1)$, and, since we will consider input flux \dot{N} and leakage rate κ in the MHz range, $\langle \Delta n_a \rangle = \mathcal{O}(G)$, which results in subleading term of $\mathcal{O}(G^2)$ in Δm_z . The $\mathcal{O}(G)$ estimate for the induced polarization will be verified numerically below (see Fig. 2d). The linearization of Eq. (22b) is justified by the same perturbative expansion.

V. QUANTUM EFFICIENCY

The detector efficiency is defined by the ratio of the steady state mean DQD current per input photon flux,

$$\eta = \frac{|\langle \Delta I \rangle|}{e\dot{N}} \quad (27)$$

where e is the electron charge, $\langle \Delta I \rangle = \langle I - I_0 \rangle$ is the mean polarization and current caused by absorbing photons and $\langle I_0 \rangle$ are the dark counts due to the current at zero photon input flux. The electron current Eq. (4) can be expressed in terms of the polarization as

$$\langle I \rangle = -\frac{e\Gamma_R(1 + m_z)}{\Gamma_{0e} + 2\Gamma_{g0}} \left(\Gamma_{0e} \cos^2 \frac{\theta}{2} - \Gamma_{g0} \sin^2 \frac{\theta}{2} \right). \quad (28)$$

As one would expect, the current is proportional the probability for the DQD to be excited, $\langle p_e \rangle = (1 + m_z)/2$. The last factor in Eq. (28) takes into account the cancellation of the left and right moving electrons.

We will henceforth consider symmetric dot-lead tunneling at the rate $\Gamma_l = \Gamma_L = \Gamma_R$. Then $\Gamma_{0e} = \Gamma_{g0} = \Gamma_l$, the photon induced current is

$$\langle \Delta I \rangle = -e \frac{\Gamma_l \cos \theta}{3} \Delta m_z, \quad (29)$$

and Eqs. (21c) and (21b) become

$$\begin{aligned} \Gamma_1 &= \gamma_1 + \frac{2\Gamma_l - \gamma_s}{3}, \\ m_0 &= -\frac{\gamma_s + \Gamma_l}{3\gamma_1/2 - \gamma_s/2 + \Gamma_l}. \end{aligned} \quad (30)$$

We will be interested in the linear regime with respect to \dot{N} , where single photon detection occurs. This regime coincides with the leading order expansion of $G\langle n_a \rangle$ in Eq. (25), where the efficiency is given by

$$\eta = \frac{4}{3} \frac{\kappa g^2 (\Gamma_l/\Gamma_1) |\cos \theta \text{Im}\chi_\sigma|}{(\Delta_{ab} - g^2|m_0|\text{Re}\chi_\sigma)^2 + (\kappa/2 + g^2|m_0|\text{Im}\chi_\sigma)^2}. \quad (31)$$

Next, we analyze quantities that characterize the DQD-resonator coupling, dissipation, and response as a function of bias, see Fig. 2a-c. As a point of reference, we show in Fig. 2a the Jaynes-Cummings energy levels in the zero and one photon subspace.

$$E_{1,\pm} = \hbar\omega_a \pm \frac{\hbar}{2} \sqrt{4g^2 + \Delta_{a\sigma}^2},$$

where $g = g_0 \sin \theta$ and we take the parameters $\omega_a/2\pi = 7$ GHz and $g_0/2\pi = 50$ MHz, which is a value that has been reported in experiments [16, 22, 48]. In Fig. 2, we choose a tunnel coupling of $t_c/2\pi = 2$ GHz, but we will optimize this parameter below. Note that, since $\Gamma_2 \gg g$, the resonances at the Jaynes-Cummings energies are destroyed; the subspace of the resonator-DQD

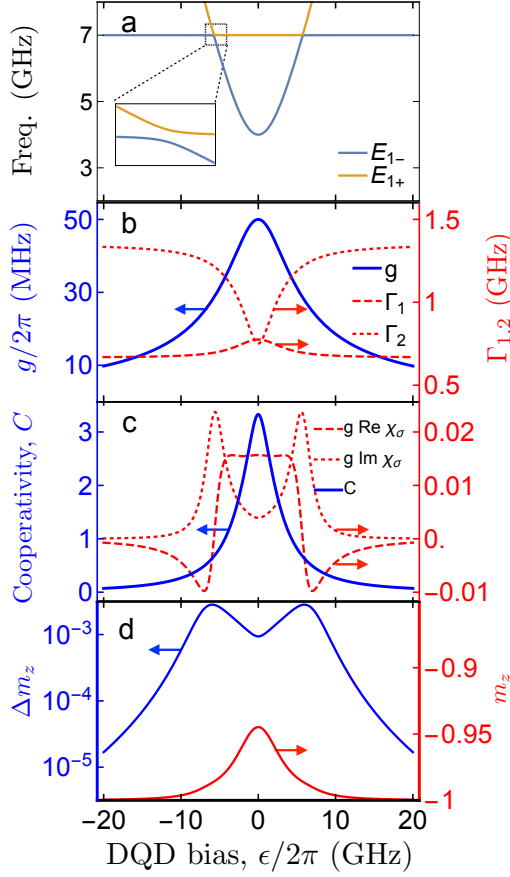


FIG. 2. As a function of the double dot bias ϵ , for $(t_c, g)/2\pi = (2, 0.05)$ GHz and $\dot{N} = 1$ MHz: (a) Jaynes-Cummings energy levels $E_{1\pm}$ of the DQD-resonator system. (b) DQD-resonator coupling $g = g_0 \sin \theta$ for $g_0/2\pi = 50$ MHz, transverse relaxation rate Γ_2 and depolarization rate Γ_1 of the effective two level DQD. (c) Cooperativity of the DQD-resonator system $C = g^2/\Gamma_2\kappa$; the real and imaginary parts of the DQD susceptibility χ_σ . (d) DQD polarization m_z and photon-induced polarization Δm_z .

system with n photons is specified by the uncoupled basis $\{|g\rangle|n\rangle, |e\rangle|n-1\rangle\}$, where $|e\rangle$ denotes the DQD excited state that is strongly broadened with a linewidth Γ_2 , as shown in Fig. 1 (lower left box).

We use DQD relaxation parameters appropriate for silicon DQD [43, 49]: phonon noise spectral density $J_{\text{ph}}/2\pi = 0.1$ GHz [cf. Eq. (A4)], quasistatic bias noise variance $\epsilon_{\text{rms}}/2\pi = 1.2$ GHz, and take dot-lead tunnel rate $\Gamma_l/2\pi = 1$ GHz. The DQD-resonator coupling g (Fig. 2b) has a broad peak centered at $\epsilon = 0$, due to a strong dipole moment at the charge degeneracy point, while the transverse relaxation rate Γ_2 has a minimum due to a sweet spot where dephasing is to the first order insensitive to quasistatic bias noise. These effects combined lead to a broad peak around $\epsilon = 0$ in the cooperativity $C = g^2/\Gamma_2\kappa$, shown in Fig. 2c, indicating strong DQD-resonator interaction. The strong charge dipole

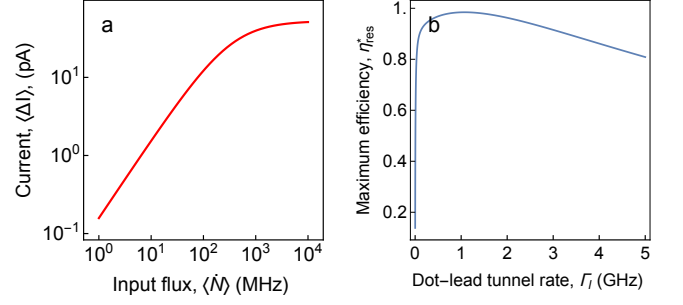


FIG. 3. For optimal parameters $\kappa/2\pi = 76$ kHz and $t_c/2\pi = 0.5$ GHz, on resonance $\Delta_{ab} = 0$: (a) Logarithmic plot of the photon-induced current $\langle \Delta I \rangle$ as a function of input flux \dot{N} for $\Gamma_l = 1$ GHz. (b) Maximum efficiency as a function of the incoherent dot-lead tunnel rate Γ_l with $\dot{N} = 1$ MHz.

also increases transitions driven by phonons and $1/f$ charge noise, leading to a peak in the equilibrium polarization of $m_0 \simeq -0.95$ at $\epsilon = 0$ (Fig. 2d) and a peak in the depolarization rate Γ_1 (Fig. 2b), which is otherwise dominated by dot-lead tunneling. The real and imaginary part of χ_σ , which modify the effective resonator frequency and decay rate, respectively, are plotted in Fig. 2c.

We conclude this section by considering the detector response as a function of input flux \dot{N} and dot-lead tunnel rate Γ_l . Nonlinear response at large flux will cause ΔI to saturate and sets the detector dead time [1]. At the same time, a sufficiently large flux is necessary for the current $\Delta I = \eta e \dot{N}$ to be measurable. Figure 3a shows the photon-induced current

$$\Delta I = 0.16\eta\dot{N} \text{ pA/MHz}$$

as a function of \dot{N} at $\Gamma_l = 1$ GHz using Eq. (37) for the optimal efficiency η_{res}^* found below. The response is linear up to $\dot{N} = 100$ MHz, and saturates as the flux approaches the effective inelastic decay rate $\dot{N} \simeq \Gamma_1$. Fig. 3b shows η_{res}^* as a function of the lead tunnel rate Γ_l at fixed $\dot{N} = 1$ MHz. The optimal rate occurs near $\Gamma_l = 1$ GHz, and is determined by the competition between two effects: when Γ_l is too low, the electron relaxes back to $|g\rangle$, but when Γ_l is too high, the efficiency suffers due to level broadening, $\Gamma_2 \propto \Gamma_l$, see Eq. (18).

Maximum photon absorption by the DQD occurs on resonance, as shown by the peaks at ϵ_{res} in the photon-induced DQD polarization Δm_z plotted in Fig. 2d, which are accompanied by minima in photon number with $n_a \lesssim 1$, indicating perfect photon to electron conversion. Note that induced polarization is very small, $\Delta m_z(\epsilon_{\text{res}}) \simeq 10^{-4} \ll m_0$, which justify our approximation of taking $m_z = m_z^0$ in Eq. (23b), and agrees with our previous estimate below Eq. (26) that $\Delta m_z = \mathcal{O}(G)$.

Figure 6a shows the photon detector efficiency as a function of bias for $\kappa = 1$ MHz, computed using Eq. (25), (27), and (29). When the charge transition is sharp, at

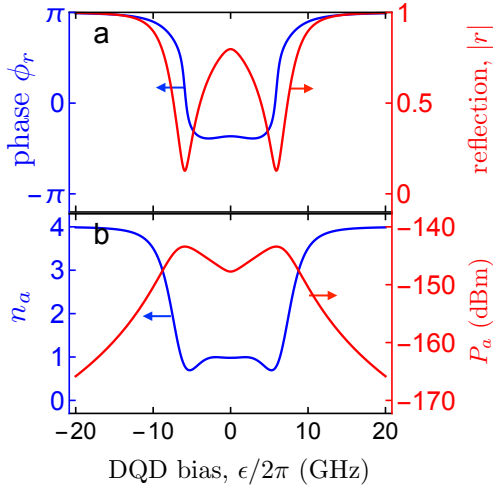


FIG. 4. As a function of the double dot bias ϵ , for $(t_c, g)/2\pi = (2, 0.05)$ GHz and $\dot{N} = 1$ MHz: (a) Magnitude $|r|$ and phase ϕ_r of the reflection coefficient. (b) Photon number n_a and power absorbed P_a .

$t_c/2\pi = 0.5$ GHz, a double-peak behavior emerges: one peak is due to resonance and the other is due to the competition between enhanced cooperativity and cancellation of left and right moving currents, which goes as $\sin^2 \theta \cos \theta$. As expected, the maximum efficiency occurs on resonance: $\eta_{\text{res}} \simeq 80\%$ at $\epsilon = \epsilon_{\text{res}}$ and $t_c/2\pi = 1.5$ GHz. This efficiency will be further optimized in section VII.

VI. REFLECTED SIGNAL

The field of the transmission line, see Eq. (12), can be described in terms of its final configuration at $t_0 = t_f > t$. In this case, we can introduce the output field as a counterpart of the input field, Eq. (13):

$$b_{\text{out}}(t) = \int_{-\infty}^{\infty} \frac{d\omega}{2\pi} b_{\omega}(t_f) e^{-i\omega(t-t_f)}. \quad (32)$$

The equation of motion for the resonator field has a structure similar to that of Eq. (17a), but an opposite sign in front of the term describing spontaneous emission:

$$\dot{a} = \left(\frac{\kappa}{2} - i\Delta_{ab} \right) a - ig\sigma + i\sqrt{\kappa}b_{\text{out}} \quad (33)$$

By subtracting the above equation from Eq. (17a), we obtain the relation between input and output modes [40],

$$b_{\text{out}}(t) = b_{\text{in}}(t) + i\sqrt{\kappa}a(t), \quad (34)$$

where on the right hand side, the first term is the reflection of the input field and the second is the field radiated by the resonator. The reflection coefficient r is defined by $b_{\text{out}} = rb_{\text{in}}$.

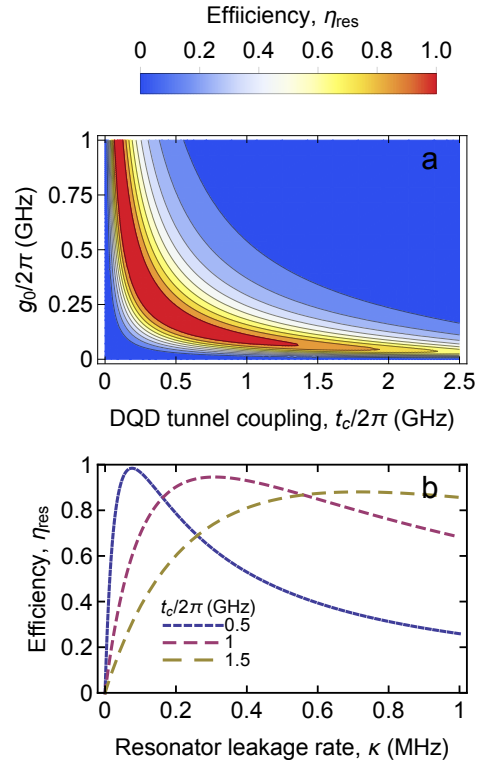


FIG. 5. (a) Photon detector efficiency on resonance η_{res} as a function of DQD-resonator coupling g_0 and interdot DQD tunnel coupling t_c , for $\kappa/2\pi = 1$ MHz. (b) Efficiency η_{res} as a function of resonator leakage rate κ .

A system of coupled DQD and microwave resonator can be also used to control the output microwave field [27, 50]. Here, we briefly analyze the suppression of the reflected signal from the resonator when the DQD device acts as an adjustable dissipating element. We consider the reflecting signal of microwave photons for input photon frequency equal to the resonator frequency, $\Delta_{ab} = 0$, and for input flux $\dot{N} = 1$ MHz, which is well within the linear regime, as shown below. In Fig. 4a, we plot the magnitude $|r|$ and phase ϕ_r of the reflection coefficient, computed by using the general relation between input and output modes Eq. (34) with a given by Eq. (23b), which yields

$$r = |r|e^{i\phi_r} = 1 + \sqrt{\kappa}\chi_{ab}. \quad (35)$$

The mean photon number $\langle n_a \rangle$ Eq. (24b) and absorbed input power $P_a = \hbar\omega_{\text{in}}(1 - |r|^2)\dot{N}$ is plotted in Fig. 4b. When the input frequency is on resonance with the DQD excitation at $\epsilon = \epsilon_{\text{res}} = \sqrt{\omega_{\text{in}}^2 - 4t_c^2}$, reflection $|r|$ is minimal and power absorption P_a is maximal.

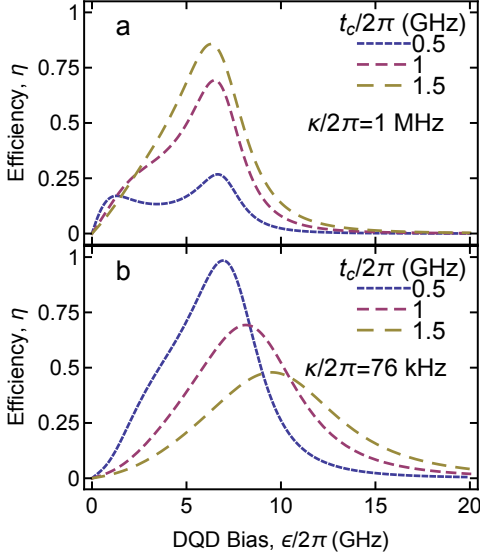


FIG. 6. Efficiency of photon detector η as a function of DQD bias ϵ , with the tunnel couplings $t_c/2\pi = (0.5, 1, 1.5)$ GHz and DQD-resonator coupling $g_0 = 50$ MHz, for (a) Nominal resonator leakage rate, $\kappa/2\pi = 1$ MHz, and (b) Optimal resonator leakage rate, $\kappa/2\pi = 76$ kHz, Eq. (36).

VII. OPTIMAL CONDITIONS

The photon detector efficiency can be further improved by reducing the reflection of input photons, which for the parameters chosen so far is nonzero even on resonance, as shown in Fig. 4a. Using Eq. (23b) and (35), we find $r(\epsilon_{\text{res}}) = 0$ when the resonator leakage rate κ matches the DQD-mediated photon dissipation rate,

$$\kappa = \frac{2(g_0 \sin \theta_{\text{res}})^2 |m_z^0|}{\Gamma_2(\epsilon_{\text{res}})}. \quad (36)$$

The latter can be understood from Fermi golden rule as a transition from the one-resonator photon state $|g\rangle|1\rangle$ to the broadened DQD excited state $|e\rangle|\emptyset\rangle$ where $|\emptyset\rangle$ denotes the empty resonator state. The factor m_0 takes into account that this transition can occur only when $|g\rangle$ ($|e\rangle$) is (un)occupied. These transitions are illustrated in Fig. 1. We note that Eq. (36) can be expressed as the condition on the cooperativity [cf. Eq. (26)]

$$C(\epsilon_{\text{res}}) = \frac{1}{2|m_0(\epsilon_{\text{res}})|} \approx \frac{1}{2},$$

so the optimal point does not require strong resonator-DQD coupling.

When Eq. (36) is satisfied, the efficiency on resonance is given by

$$\eta_{\text{res}}^* = |\cos \theta_{\text{res}}| \frac{2\Gamma_l/3\Gamma_1}{1 + 2\tilde{N}/|m_0|\Gamma_1}. \quad (37)$$

For a sufficiently fast dot-lead tunnel rate $\Gamma_l \gg \gamma_{\uparrow,\downarrow}$, $\Gamma_1 \simeq 3\Gamma_l/2$, see Eq. (30), so that η_{res} is limited mainly by the factor

$$|\cos \theta_{\text{res}}| = \sqrt{1 - 4t_c^2/\omega_{\text{in}}^2}. \quad (38)$$

Higher maximum efficiency η_{res} can be thus achieved by lowering t_c , but at the cost of increasing the optimal coupling g_0^* , due to the reduction in the DQD-resonator coupling by $\sin \theta_{\text{res}} = 2t_c/\omega_{\text{in}}$. This behavior is shown in Fig. 5a, where we plot efficiency on resonance η_{res} as a function of t_c and g_0 .

The optimal regime defined by Eq. (36) can be reached by tuning DQD-resonator parameters t_c , g_0 , and κ . At $\kappa = 1$ MHz, it can be satisfied at $(t_c, g_0^*) \simeq 2\pi(0.5, 0.2)$ GHz, but this g_0^* is larger than presently available DQD-resonator couplings. We therefore propose lowering the resonator leakage rate κ at fixed g_0 . Fig. 5b shows η_{res}^* plotted as a function of κ for several values of t_c . The maximum efficiency is $\eta_{\text{max}} = 98.4\%$ and occurs at $\kappa^*/2\pi = 76$ kHz and $t_c/2\pi = 0.5$ GHz. We note that this value of κ^* is well within the range of three-dimensional superconducting resonators which can have leakage rates as low as $\kappa = 0.1$ kHz [51]. Fig. 6b shows the detector efficiency as a function of DQD bias in the optimal regime.

VIII. CONCLUSIONS AND DISCUSSION

In summary, we have theoretically proposed and optimized a microwave photon detector based on a resonator-coupled double quantum dot, which could readily be integrated with current cQED technology. We show that very high quantum efficiency is possible with currently achievable values of the DQD-resonator coupling and DQD dissipation, and determined the parameter regime for near-unit efficiency. While we utilized purely charge states of the DQD in this work, our theoretical model can readily be applied to spin-charge hybridized DQD states, for example, the singlet and triplet states of Ref. [52], which are protected from charge noise dephasing and hence advantages for applications in quantum communication.

The proposed photon detector allows measurements of the input photon statistics as well, so that one could distinguish pure input Fock states from classical states by measuring the second order photon correlation [39]. However, determining the exact relation between photon and electric current noise is beyond the scope of this paper. To address this relation, one has to analyze the effect of fluctuations in the resonator photon number due to fluctuations in \tilde{N} , which results in σ_z and current fluctuations and also in the backaction of the DQD on the resonator photons. Note also that multi-photons states with k photons in the resonator can also be detected by tuning the DQD to resonance with $k\omega_{\text{in}}$, but results in weaker signal since the multi-photon absorption transition amplitudes are reduced by the factor g^k at weak coupling [53].

ACKNOWLEDGMENTS

We are thankful to R. McDermott, B. Plourde, M. Schoendorf, F. Wilhelm, and C. Xu for fruitful discussions. M.V. was supported by the Army Research Office under contract W911NF-14-1-0080 and NSF Grant No. DMR 0955500. C.W. was supported by the Intelligence Community Postdoctoral Research Fellowship Program.

Appendix A: DQD depolarization and dephasing rates

In this section, we discuss dependence on the DQD bias ϵ of the total DQD depolarization rate γ_1 , the spontaneous relaxation rate γ_s , and the charge noise induced pure dephasing γ_ϕ . The depolarization rate is the sum of the relaxation and excitation rates $\gamma_1 = \gamma_\uparrow + \gamma_\downarrow$ and originates due to variety of processes including electron-phonon interactions and bias noise contributions. Because charge noise and phonons couple to the DQD charge dipole matrix element, the associated relaxation is proportional $\sin^2 \theta = 4t_c^2/\omega_\sigma^2$, leading to the peak in γ_1 and γ_s at $\epsilon = 0$. In contrast, bias noise induced pure dephasing is strongest at large ϵ where the DQD frequency ω_σ is more sensitive to bias noise $\delta\epsilon$, and smallest at $\epsilon = 0$ where the DQD energy is first order insensitive to bias noise. The physical reason for this dependence on ϵ is that at large ϵ the DQD eigenstates are pure charge states $|L\rangle$ or $|R\rangle$, while at the charge transition $\epsilon = 0$ the eigenstates are fully hybridized charge states $(|L\rangle \pm |R\rangle)/\sqrt{2}$. The qualitative bias dependence of Γ_2 [cf, Eq. (18)] follows that of γ_ϕ , since the dip in γ_ϕ near $\epsilon = 0$ is typically greater than the peak in γ_1 .

Below we describe the minimal phenomenological model we used to incorporate phonons and charge noise in the DQD dissipation and decoherence, and provide explicit formulas for the relaxation rates $\gamma_{\uparrow,\downarrow}^{\text{ph}}$, γ_1^{ch} , γ_s , and γ_ϕ . Using these formulas, we plot γ_1 , γ_s , and γ_ϕ as a function of in Fig. 7 for the following choice of parameters: DQD frequency $\omega_\sigma/2\pi = 7$ GHz, DQD-resonator coupling $g_0/2\pi = 50$ MHz, phonon noise spectral density $J_{\text{ph}}/2\pi = 0.1$ GHz, temperature $T = 50$ mK, quasistatic bias noise variance $\epsilon_{\text{rms}}/2\pi = 1.2$ GHz, and $1/f$ noise strength $c_\epsilon = 2.4$ μeV .

1. Relaxation rates due to phonons

The electron-phonon interaction Hamiltonian can be written as [54]

$$H_{\text{ph}} = \sin \theta \sum_{\mathbf{k}\lambda} \beta_{\mathbf{k}\lambda} (\sigma^\dagger a_{\mathbf{k}\lambda} + a_{\mathbf{k}\lambda}^\dagger \sigma), \quad (\text{A1})$$

where λ labels the phonon branches,

$$\beta_{\mathbf{k}\lambda} = v_{\mathbf{k}\lambda} \int d\mathbf{r} e^{i\mathbf{k}\cdot\mathbf{r}} \frac{|\phi_L(\mathbf{r})|^2 - |\phi_R(\mathbf{r})|^2}{2}$$

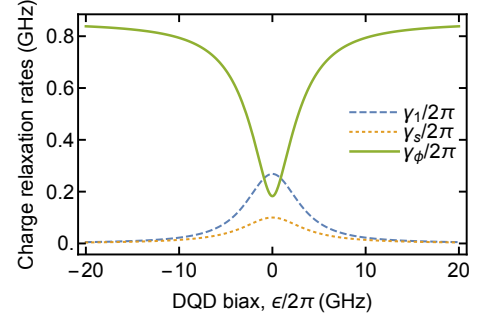


FIG. 7. The DQD charge relaxation rates, T_1 relaxation rate γ_1 , difference in excitation and relaxation rates due to thermal phonons γ_s , and quasistatic dephasing rate due to charge noise γ_ϕ as a function of the DQD bias ϵ .

where $\phi_i(\mathbf{r})$, are the localized (wannier) basis functions for the DQD electrons, and $v_{\mathbf{k}\lambda}$ are coupling coefficients that depends on phonon parameters [55].

From Fermi's golden rule, the stimulated emission and absorption rates are given by

$$\begin{pmatrix} \gamma_\uparrow^{\text{ph}} \\ \gamma_\downarrow^{\text{ph}} \end{pmatrix} = \gamma_s \begin{pmatrix} n_{\text{ph}}(\omega_\sigma) \\ 1 + n_{\text{ph}}(\omega_\sigma) \end{pmatrix} \quad (\text{A2})$$

where $n_{\text{ph}}(\omega) = (e^{\hbar\omega/k_B T} - 1)^{-1}$ is the phonon thermal distribution. The phonon-induced spontaneous emission rate is given by

$$\gamma_s = \sin^2 \theta J_{\text{ph}}(\omega_\sigma), \quad (\text{A3})$$

$$\text{where } J_{\text{ph}}(\omega) = 2\pi \sum_{\mathbf{k}\lambda} |\beta_{\mathbf{k}}|^2 \delta(\omega - \omega_{\mathbf{k}\lambda}^{\text{ph}}) \quad (\text{A4})$$

is the phonon spectral density and $\omega_{\mathbf{k}\lambda}^{\text{ph}}$ are the phonon dispersions. We assume a typical temperature of 50 mK. Note that phonons do not cause pure dephasing due to the vanishing phonon density of states at zero frequency [56].

The phonon spectrum is material dependent. For silicon quantum dots, Ref. [43] measures a charge relaxation times of up to 10 ns at the DQD excitation frequency $\omega_\sigma/2\pi = 12$ GHz with the tunnel coupling $2t_c = 5.9$ GHz. We take a nominal value of $J_{\text{ph}}(\omega) = 0.1$ GHz.

2. Relaxation rates due to charge noise

We assume a $1/f$ charge noise spectrum

$$S_\epsilon(\omega) = \frac{c_\epsilon^2}{|\omega|}, \quad \omega_l < |\omega| < \omega_h, \quad (\text{A5})$$

where $c_\epsilon = 2.4$ μeV [57]. The depolarization rate is given by [58]

$$\frac{\gamma_1^{\text{ch}}(\epsilon)}{2\pi} = \sin^2 \theta \frac{S_\epsilon(\omega_\sigma)}{2\hbar^2}. \quad (\text{A6})$$

If the subsystem that produces this noise is thermal at the low temperature, spontaneous relaxation rate $\gamma_s^{\text{ch}}(\epsilon)$ due to this noise would coincide with $\gamma_1^{\text{ch}}(\epsilon)$. In case if the source of the noise is a high-temperature environment, we expect $\gamma_s^{\text{ch}}(\epsilon) \ll \gamma_1^{\text{ch}}(\epsilon)$.

The low frequency part of the noise spectrum causes

quasistatic fluctuations $\delta\omega_\sigma$ of the DQD excitation frequency. The associated dephasing rate is given by [57]

$$\frac{\gamma_\phi}{2\pi} = \sqrt{\left(\frac{\partial\omega_\sigma}{\partial\epsilon} \frac{\epsilon_{\text{rms}}}{\sqrt{2}}\right)^2 + \left(\frac{\partial^2\omega_\sigma}{\partial\epsilon^2} \frac{\epsilon_{\text{rms}}^2}{2}\right)^2} \quad (\text{A7})$$

-
- [1] R. H. Hadfield, Nat Photon **3**, 696 (2009).
 - [2] Y. Nakamura, in *Photonics Conference (IPC), 2012 IEEE* (2012) pp. 544–545.
 - [3] Y. Nakamura and T. Yamamoto, Photonics Journal, IEEE **5**, 0701406 (2013).
 - [4] H. Spieler, Nuclear Instruments and Methods in Physics Research Section A: Accelerators, Spectrometers, Detectors and Associated Equipment **531**, 1 (2004), proceedings of the 5th International Workshop on Radiation Imaging Detectors.
 - [5] B. Peropadre, G. Romero, G. Johansson, C. M. Wilson, E. Solano, and J. J. García-Ripoll, Phys. Rev. A **84**, 063834 (2011).
 - [6] Y.-F. Chen, D. Hover, S. Sendelbach, L. Maurer, S. T. Merkel, E. J. Pritchett, F. K. Wilhelm, and R. McDermott, Phys. Rev. Lett. **107**, 217401 (2011).
 - [7] G. Romero, J. J. García-Ripoll, and E. Solano, Phys. Rev. Lett. **102**, 173602 (2009).
 - [8] K. Koshino, K. Inomata, T. Yamamoto, and Y. Nakamura, Phys. Rev. Lett. **111**, 153601 (2013).
 - [9] K. Koshino, K. Inomata, Z. Lin, Y. Nakamura, and T. Yamamoto, Phys. Rev. A **91**, 043805 (2015).
 - [10] A. Poudel, R. McDermott, and M. G. Vavilov, Phys. Rev. B **86**, 174506 (2012).
 - [11] S. Barzanjeh, M. C. de Oliveira, and S. Pirandola, ArXiv e-prints (2014), arXiv:1410.4024 [quant-ph].
 - [12] S. Barzanjeh, S. Guha, C. Weedbrook, D. Vitali, J. H. Shapiro, and S. Pirandola, Phys. Rev. Lett. **114**, 080503 (2015).
 - [13] K. Zhang, F. Bariani, Y. Dong, W. Zhang, and P. Meystre, Phys. Rev. Lett. **114**, 113601 (2015).
 - [14] G.-W. Deng, L. Henriët, D. Wei, S.-X. Li, H.-O. Li, G. Cao, M. Xiao, G.-C. Guo, M. Schiro, K. Le Hur, and G.-P. Guo, ArXiv e-prints (2015), arXiv:1509.06141 [cond-mat.mes-hall].
 - [15] G.-W. Deng, D. Wei, S.-X. Li, J. R. Johansson, W.-C. Kong, H.-O. Li, G. Cao, M. Xiao, G.-C. Guo, F. Nori, H.-W. Jiang, and G.-P. Guo, Nano Letters **15**, 6620 (2015).
 - [16] G.-W. Deng, D. Wei, J. R. Johansson, M.-L. Zhang, S.-X. Li, H.-O. Li, G. Cao, M. Xiao, T. Tu, G.-C. Guo, H.-W. Jiang, F. Nori, and G.-P. Guo, Phys. Rev. Lett. **115**, 126804 (2015).
 - [17] M.-L. Zhang, D. Wei, G.-W. Deng, S.-X. Li, H.-O. Li, G. Cao, T. Tu, M. Xiao, G.-C. Guo, H.-W. Jiang, and G.-P. Guo, Applied Physics Letters **105**, 073510 (2014).
 - [18] J. Basset, D.-D. Jarausch, A. Stockklauser, T. Frey, C. Reichl, W. Wegscheider, T. M. Ihn, K. Ensslin, and A. Wallraff, Phys. Rev. B **88**, 125312 (2013).
 - [19] M. Kulkarni, O. Cotlet, and H. E. Türeci, Phys. Rev. B **90**, 125402 (2014).
 - [20] C. Xu and M. G. Vavilov, Phys. Rev. B **87**, 035429 (2013); Phys. Rev. B **88**, 195307 (2013).
 - [21] K. D. Petersson, L. W. McFaul, M. D. Schroer, M. Jung, J. M. Taylor, A. A. Houck, and J. R. Petta, Nature **490**, 380 (2012).
 - [22] T. Frey, P. J. Leek, M. Beck, A. Blais, T. Ihn, K. Ensslin, and A. Wallraff, Phys. Rev. Lett. **108**, 046807 (2012).
 - [23] P.-Q. Jin, M. Marthaler, J. H. Cole, A. Shnirman, and G. Schön, Phys. Rev. B **84**, 035322 (2011).
 - [24] L. Childress, A. S. Sørensen, and M. D. Lukin, Phys. Rev. A **69**, 042302 (2004).
 - [25] Y.-Y. Liu, K. D. Petersson, J. Stehlik, J. M. Taylor, and J. R. Petta, Phys. Rev. Lett. **113**, 036801 (2014).
 - [26] Y.-Y. Liu, J. Stehlik, C. Eichler, M. J. Gullans, J. M. Taylor, and J. R. Petta, Science **347**, 285 (2015).
 - [27] M. Schiró and K. Le Hur, Phys. Rev. B **89**, 195127 (2014).
 - [28] A. D. Greentree, C. Tahan, J. H. Cole, and L. C. L. Hollenberg, Nat Phys **2**, 856 (2006).
 - [29] K. Le Hur, L. Henriët, A. Petrescu, K. Plekhanov, G. Roux, and M. Schiró, (2015), arXiv:1505.00167.
 - [30] J. I. Cirac, P. Zoller, H. J. Kimble, and H. Mabuchi, Phys. Rev. Lett. **78**, 3221 (1997).
 - [31] D. Pinotsi and A. Imamoglu, Phys. Rev. Lett. **100**, 093603 (2008).
 - [32] M. G. Vavilov and A. D. Stone, Phys. Rev. Lett. **97**, 216801 (2006).
 - [33] C. Bergenfeldt, P. Samuelsson, B. Sothmann, C. Flindt, and M. Büttiker, Phys. Rev. Lett. **112**, 076803 (2014).
 - [34] S. A. Gurvitz and Y. S. Prager, Phys. Rev. B **53**, 15932 (1996).
 - [35] A. B. Vorontsov and M. G. Vavilov, Phys. Rev. Lett. **101**, 226805 (2008).
 - [36] The resonator mode a is dimensionless, while the transmission line modes have units of $b_\omega \sim \sqrt{\text{time}}$ and $b_{\text{in}}(t) \sim 1/\sqrt{\text{time}}$.
 - [37] C. Gardiner and P. Zoller, *Quantum Noise: A Handbook of Markovian and Non-Markovian Quantum Stochastic Methods with Applications to Quantum Optics*, Springer Series in Synergetics (Springer, New York, NY, USA, 2004).
 - [38] M. J. Collett and C. W. Gardiner, Phys. Rev. A **30**, 1386 (1984).
 - [39] D. Walls and G. Milburn, *Quantum Optics*, Springer Study Edition (Springer Berlin Heidelberg, 2012).
 - [40] A. A. Clerk, M. H. Devoret, S. M. Girvin, F. Marquardt, and R. J. Schoelkopf, Reviews of Modern Physics **82**, 1155 (2010).
 - [41] B. Q. Baragiola, R. L. Cook, A. M. Brańczyk, and J. Combes, Phys. Rev. A **86**, 013811 (2012).
 - [42] X. Hu and S. Das Sarma, Phys. Rev. Lett. **96**, 100501 (2006).
 - [43] K. Wang, Phys. Rev. Lett. **111**, 046801 (2013).
 - [44] W. A. Coish and D. Loss, Phys. Rev. B **70**, 195340

- (2004).
- [45] C. Buizert, F. H. L. Koppens, M. Pioro-Ladrière, H.-P. Tranitz, I. T. Vink, S. Tarucha, W. Wegscheider, and L. M. K. Vandersypen, *Phys. Rev. Lett.* **101**, 226603 (2008).
 - [46] O. E. Dial, M. D. Shulman, S. P. Harvey, H. Bluhm, V. Umansky, and A. Yacoby, *Phys. Rev. Lett.* **110**, 146804 (2013).
 - [47] When $\langle b_{\text{in}} \rangle \neq 0$, we have to keep the term $\langle a \rangle \sigma_z$ in the equation for σ .
 - [48] J. J. Viennot, M. R. Delbecq, M. C. Dartiailh, A. Cottet, and T. Kontos, *Phys. Rev. B* **89**, 165404 (2014).
 - [49] K. D. Petersson, J. R. Petta, H. Lu, and A. C. Gossard, *Phys. Rev. Lett.* **105**, 246804 (2010).
 - [50] M. Goldstein, M. H. Devoret, M. Houzet, and L. I. Glazman, *Phys. Rev. Lett.* **110**, 017002 (2013).
 - [51] M. Reagor, H. Paik, G. Catelani, L. Sun, C. Axline, E. Holland, I. M. Pop, N. A. Masluk, T. Brecht, L. Frunzio, M. H. Devoret, L. Glazman, and R. J. Schoelkopf, *Applied Physics Letters* **102**, 192604 (2013).
 - [52] C. H. Wong, M. A. Eriksson, S. N. Coppersmith, and M. Friesen, *Phys. Rev. B* **92**, 045403 (2015).
 - [53] W. G. van der Wiel, S. De Franceschi, J. M. Elzerman, T. Fujisawa, S. Tarucha, and L. P. Kouwenhoven, *Rev. Mod. Phys.* **75**, 1 (2002).
 - [54] G. Mahan, *Many-Particle Physics*, Physics of Solids and Liquids (Springer, 2000).
 - [55] M. J. Gullans, Y.-Y. Liu, J. Stehlik, J. R. Petta, and J. M. Taylor, *Phys. Rev. Lett.* **114**, 196802 (2015).
 - [56] X. Hu, *Phys. Rev. B* **86**, 035314 (2012).
 - [57] C. H. Wong, *Phys. Rev. B* **93**, 035409 (2016).
 - [58] Y. Makhlin, G. Schön, and A. Shnirman, *Chemical Physics* **296**, 315 (2004).